International Journal of GEOMATE, Oct., 2025 Vol.29, Issue 134, pp.120-132
ISSN: 2186-2982 (P), 2186-2990 (O), Japan, DOI: https://doi.org/10.21660/2025.134.5090
Geotechnique, Construction Materials and Environment

RESEARCH ON STATIC MECHANICAL PROPERTIES AND MICROSTRUCTURE OF COMPOSITE RUBBER CEMENT MORTAR BASED ON ORTHOGONAL EXPERIMENTS

Chunyi WANG[a], Tingjie WU[a], *Xiangqin DU[a], Zhilong LIU[a], Meimei LEI[a], Rongfei CHEN[a]

[a] College of Material and Architectural Engineering, Guizhou Normal University, Guiyang 550025, China

*Corresponding Author, Received: 18 June 2025, Revised: 15 July 2025, Accepted: 19 July 2025

ABSTRACT: An L16 (4×4) orthogonal experiment was conducted to investigate the effect of rubber particle size, rubber content, fly ash content, and silica fume content on the fluidity and mechanical properties of composite rubber mortar, and the corresponding mechanisms were explored. The results indicated that silica fume exhibited the dominant influence on the fluidity of composite rubber mortar, while the rubber content demonstrated the most significant impact on the compressive strength, flexural strength, and flexural-compression ratio of rubber mortar. As the curing age increased, the reinforcing effect of fly ash and silica fume on the compressive and flexural strength of composite rubber mortar became more pronounced, indicating that an appropriate amount of fly ash and silica fume exerted a positive synergistic effect on the mechanical strength of composite rubber mortar. Furthermore, both fly ash and silica fume can improve the weak interfacial transition zone (ITZ) caused by rubber incorporation. This improvement leads to a denser pore structure in the composite rubber mortar. As a result, the enhanced mechanical properties significantly reduce the strength loss induced by rubber. Through orthogonal experimental analysis, the optimal combination A1B1C4D2 was identified, corresponding to a rubber particle size of 150 mesh, rubber content of 5%, fly ash content of 20%, and silica fume content of 5%. This specific formulation demonstrated the most favorable comprehensive performance characteristics for the composite rubberized mortar.

Keywords: Composite rubber mortar; Rubber; Fly ash; Silica fume; Mechanical properties

1. INTRODUCTION

Energy saving and emission reduction have become the focus of international attention, and building materials play a crucial role in the process of global warming and the realization of the “dual-carbon” goal [1]. With the rapid development of the automotive industry, large quantities of waste tires and rubber products have accumulated, which not only occupy land resources and causes pollution, but also create environmental hazards due to their non-degradable nature [2]. Scholars have found that the rubber cementitious materials made by mixing waste rubber into concrete as powder or granules show better fatigue resistance, vibration damping, noise reduction, and energy absorption capability than conventional concrete [3-5]. These materials show great potential for application in the field of roads, bridges, and water conservancy engineering [6]. At the same time, fly ash (FA) and silica fume (SF) can be used as cement substitutes in practical applications, reducing the amount of cement clinker, lowering carbon emissions in the cement production process, and realizing the efficient use of resources [7].

Although rubber cementitious materials have achieved efficient utilization of resources, studies have shown that the strength of rubber concrete decreases significantly as the rubber content increases [8]. Hilal et al. showed that an increase in rubber content led to a decrease in the compressive strength of concrete, with a more pronounced decline as the rubber particle size increased [9]. Zhu et al. stated that when the volume rate of rubber was increased from 5% to 15%, the compressive and flexural strengths of fiber rubber concrete blended from lava rock and polypropylene decreased by 5.84% and 4.63%, respectively [10]. Gupta et al. noted that the presence of microscopic cracks within the rubber weakened the bond strength between the rubber and the cement paste interface, resulting in a substantial decline in the strength of rubber concrete [11]. Fly ash and silica fume, as solid waste materials, can improve the interfacial transition zone of concrete, refine the pore structure, and enhance the mechanical properties of concrete. Incorporation of mineral admixtures such as fly ash and silica fume into rubber mortar holds promise for improving its mechanical performance. Guo et al. found that replacing cement with 10% fly ash and 20% slag increased the compressive strength, initial fracture toughness, unstable fracture toughness, and fracture energy by 23.9%, 25.2%, 45.3%, and 22.6%, respectively, when compared to ordinary concrete [12]. Zhang et al. pointed out that when the rubber particle size of 60 mesh and silica fume content of 8% were incorporated, the compressive strength was only reduced by 3. 08 MPa compared to ordinary cement

mortar, fully demonstrating the superior performance of silica fume content to improve the rubber mortar [13]. Nežerka et al. pointed out that concrete could obtain higher strength by mixing an appropriate amount of silica fume and fly ash [14].

Rubber, fly ash, and silica fume all affect the mechanical properties of mortar. However, most of the reported research on the effect of rubber on the mechanical properties of cement mortar focuses primarily on different dosages and particle sizes. The combined effect of rubber, fly ash, and silica fume in mortar, along with its impact on the mechanical properties of the matrix and the underlying mechanisms, is rarely reported. This study analyzes the effects of rubber particle size and content, fly ash content, and silica fume content on the static mechanical properties of composite rubber mortar and its mechanism and determines the optimal combination through L16 (4×4) orthogonal experiment design.

To systematically present this research, the remainder of the paper is structured as follows: Section 2 outlines the research background. Section 3 details the experimental materials and methodologies. Section 4 first employs range analysis and analysis of variance (ANOVA) to systematically examine the effects of rubber , fly ash, and silica fume dosages on mortar fluidity, compressive strength, flexural strength, and the ratio of flexural strength to compressive strength. Subsequently, the technique for order preference by similarity to ideal solution (TOPSIS) is applied to determine the optimal mixture proportion. The economic cost savings achieved by replacing fine aggregates with rubber and cement with FA/SF under this optimal proportion are quantitatively evaluated. Finally, mercury intrusion porosimetry (MIP) and scanning electron microscopy (SEM) analyses are integrated to elucidate the mechanisms underlying macroscopic mechanical property variations at the microscale. Section 5 summarizes the core conclusions. Section 6 acknowledges the funding support. Section 7 provides the reference list.

2. RESEARCH SIGNIFICANCE

This study innovatively employs an L16 orthogonal array design to investigate the synergistic effects of crumb rubber particles and mineral admixtures (fly ash and silica fume) on the workability, compressive strength, flexural strength, and flexural-compressive strength ratio of cement mortar. The research not only enriches the theoretical framework for rubber gradation optimization but also elucidates the multi-scale synergistic mechanisms between fly ash and silica fume, particularly in terms of microstructural modification and interfacial transition zone enhancement. Experimental results demonstrate that the coordinated interaction of fly ash and silica fume effectively mitigates the strength reduction induced by rubber incorporation while significantly improving mortar toughness, thereby achieving an optimal balance between mechanical performance and ductility.

In terms of environmental benefits, this study achieves efficient recycling of industrial wastes by synergistically utilizing waste rubber, fly ash, and silica fume. It significantly reduces cement consumption, thereby lowering energy use and carbon emissions during cement production. Additionally, it effectively mitigates environmental issues such as soil pollution from landfilled rubber and air pollution caused by fly ash stockpiling. The optimized mixture ratio derived from orthogonal experimental design provides a scientific basis for developing eco-friendly mortar with superior mechanical properties and maximized waste incorporation. These findings offer practical solutions for promoting sustainable development in the construction industry.

3. MATERIALS AND METHODS

3.1 Materials

The cement used was P.O. 42.5 Portland cement (equivalent to ASTM Type I), complying with Chinese standard GB/T 14684-2022. Manufactured sand with a fineness modulus of 2.85 served as fine aggregate. Technical properties of rubber are listed in Table 1. Fly ash conforming to Grade I was employed, exhibiting a density of 2.55 g/cm^3. Silica fume contained 96.20% SiO_2 with a specific surface area of 19.1 m^2/g. Major chemical compositions of fly ash and silica fume are provided in Table 2.

3.2 Specifications

L16 (4×4) orthogonal experiment was used to study the effects of four factors rubber particle size, rubber content, fly ash content, and silica fume content on the performance of composite rubber mortar, and the orthogonal test factors and level distribution are shown in Table 3. Numbers A, B, C, and D represent rubber particle size, rubber content, fly ash content, and silica fume content respectively. The rubber particle sizes used were 150 mesh (0.1 mm), 40 mesh (0.425 mm), 20 mesh (0.85 mm), and 10 mesh (2.0 mm), which replaced the mechanism sand at 5%, 10%, 15%, and 20% volume substitution rates, respectively. Fly ash and silica fume replaced cement at replacement levels of 5%, 10%, 15%, and 20% and 3%, 5%, 9%, and 15% by mass, respectively. Cement-only mortar (OM) served as the reference. The sand-binder ratio was maintained at 1:2.5 and the water-binder ratio at 0.5 throughout the experiments. Table 4 details the experimental mix proportions.

Table 1. Technical index of rubber particles

Screening rate/%	Metal content/%	Fiber content/%	Water content/%	Ash content/%	Acetone extract/%
91	0.02	0.38	0.6	6	15

Table 2. The main chemical composition of fly ash and silica fume

Material	Mass fraction/%						
	SiO_2	Al_2O_3	CaO	SO_3	Fe_2O_3	MgO	Loss on ignition
Fly ash	43.00	23.00	5.60	0.80	2.50	0.95	3.10
Silica fume	96.20	0.31	0.10	—	0.07	0.11	3.92

Table 3. Level table of orthogonal test factors

Level	Factor			
	Rubber particle size/mesh (A)	Rubber content/% (B)	Fly ash content/% (C)	Silica fume content/% (D)
1	150	5	5	3
2	40	10	10	5
3	20	15	15	9
4	10	20	20	15

Table 4. Mix the proportion of mortar

Sample	Mix proportion/g					
	Sand	Water	Cement	Rubber content	Fly ash content	Silica fume content
OM	1250.0	250	500	—	—	—
A1B1C4D2	1187.5	250	375	25.4	100	25
A1B2C3D1	1125.0	250	410	50.7	75	15
A1B3C2D4	1062.5	250	375	76.1	50	75
A1B4C1D3	1000.0	250	430	101.5	25	45
A2B1C2D3	1187.5	250	405	25.4	50	45
A2B2C1D4	1125.0	250	400	50.7	25	75
A2B3C4D1	1062.5	250	385	76.1	100	15
A2B4C3D2	1000.0	250	400	101.5	75	25
A3B1C3D4	1187.5	250	350	25.4	75	75
A3B2C4D3	1125.0	250	355	50.7	100	45
A3B3C1D2	1062.5	250	450	76.1	25	25
A3B4C2D1	1000.0	250	435	101.5	50	15
A4B1C1D1	1187.5	250	460	25.4	25	15
A4B2C2D2	1125.0	250	425	50.7	50	25
A4B3C3D3	1062.5	250	380	76.1	75	45
A4B4C4D4	1000.0	250	325	101.5	100	75

3.3 Specimen preparation and maintenance

Fly ash, silica fume, cement, and water were first mixed to prepare a cement paste, and then the rubber and sand were mixed uniformly. Specimens of 40 mm×40 mm×160 mm were prepared following standard procedures. After one day of curing at room temperature, the specimens were demolded and then cured at (20 ± 2)°C and relative humidity (RH) ≥ 95% for 7, 28, and 90 days. The experimental procedure and fluidity measurement are illustrated in Fig. 1 (a) and Fig. 1 (b), respectively.

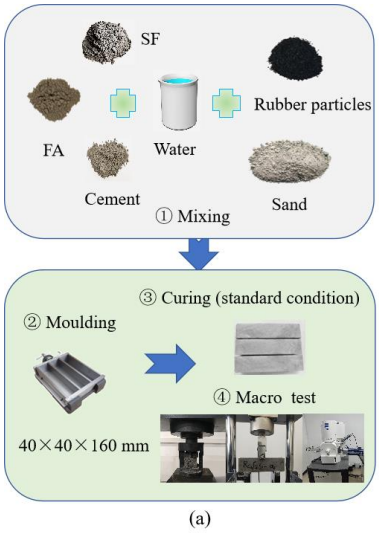

(a)

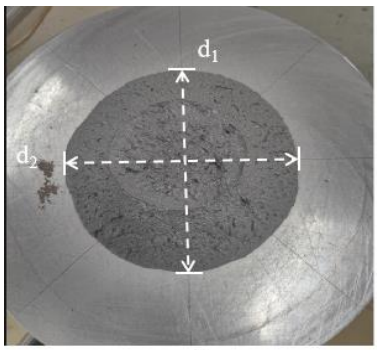

(b)

Fig. 1 Specimen preparation and testing: (a) Flow chart of experiment; (b) Tests of fluidity

4. RESULTS AND DISCUSSION

4.1 Range analysis

4.1.1 Fluidity

Range analysis results of the fluidity of the composite rubber mortar are presented in Table 5. Based on R-values, the order of the influence of each factor on its fluidity is considered to be D>B>A>C, with silica fume content having the most significant influence on the fluidity. The average value of the fluidity factor of the composite rubber mortar is shown in Fig. 2. It can be observed that as the silica fume content increased from 3% to 15%, the fluidity of the composite rubber mortar showed a tendency to increase first and then decrease sharply. When the silica fume content was 3%, the fluidity improved by 4.5% compared with that of the OM group (198 mm). However, when the silica fume content reached 15%, the fluidity decreased by 32.9% compared with that of the OM group. This trend can be attributed to the micro-aggregate filling effect and a ball effect of silica fume, which enhance the compactness of the mortar at appropriate dosages, thereby improving fluidity [15]. On the other hand, due to the large specific surface area of silica fume, its high water demand leads to a sharp reduction in fluidity as the silica fume content continues to increase, and the excess of silica fume resulted in the reduction of fluidity [16-17]. As shown in Fig. 2, A3B1C3D1 is most favorable for construction because of its best fluidity.

Table 5. Results of the range analysis for the fluidity

Projects	Fluidity/mm			
	Factor A	Factor B	Factor C	Factor D
Kavg value	182	185	180	201
	181	181	175	196
	184	184	186	164
	171	171	178	159
R	12	13	11	42

Note: Kavg value indicates the mean value of the results of each level of test under the same factor; R represents the range of factors, and the R-value can be used to evaluate the relative influence of each factor.

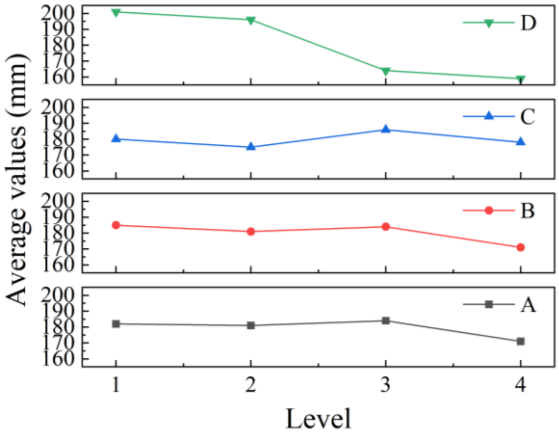

Fig. 2 The average value of the fluidity factor of composite rubber mortar

4.1.2 Compressive strength

The range analysis results for compressive strength at curing ages of 7, 28, and 90 days are shown in Table 6. Based on the R-values, the

influence of each factor on the 7-day compressive strength is ranked as B>D>A>C, the influence of the 28-day compressive strength is ranked as B>D>C>A, and the compressive strength of the 90-day compressive strength is ranked as B>D>C>A.

Multi-age studies reveal the stage-dependent characteristics of compressive strength development in rubberized mortar. At 7 days, cement hydration dominates the strength development, while the weak ITZ formed by rubber particles generate new micro-pores and micro-cracks, leading to early-age strength reduction. At 28 days, the pozzolanic reactions of fly ash and silica fume contribute to pore structure refinement, partially compensating for the negative effects of rubber incorporation. Until 90 days, cement hydration is essentially complete, continued pozzolanic reactions further optimize the microstructure, while the interfacial damage caused by rubber particles stabilizes. Quantitative analysis demonstrates that the positive effects of mineral admixtures (with range values R of 4.95 and 1.90 at 28 and 90 days, respectively) outweigh the negative impact of rubber (R values of 2.82 and 1.45), confirming their compensatory effect on compressive strength [18]. This multi-component system demonstrates a dynamic balance between hydration, interfacial bonding, and pore refinement, offering practical insights for material design.

Fig. 3 shows the average values of the 90-day compressive strength of composite rubber mortar. It can be observed that the compressive strength decreased with the increase of rubber particle size, and gradually increased with the addition of fly ash and silica fume. When the rubber content increased from 5% to 20%, its compressive strength decreased by 43.63%. This reduction is primarily attributed to the decreased sand content in the composite rubber mortar, which plays a supporting role in the compressive test. The addition of rubber makes this supporting role weakened [19]. Additionally, the surface of the rubber particles tends to form a porous structure, which leads to easy formation of microcracks around them, and the adhesion between rubber particles and cement matrix is weakened [20]. Consequently, the compressive strength of the composite rubber mortar declines. Both fly ash and silica fume are mineral admixtures exhibiting the “pozzolanic effect”. Their combined incorporation improves the ITZ between cement and aggregates, refines the pore structure of cement mortar, and optimizes pore size distribution, thereby enhancing compactness. This leads to a more uniform stress distribution within the specimens, ultimately improving compressive strength [21]. These effects lead to a more uniform stress distribution when the mortar specimen is subjected to stress, and the increase in compressive strength is inevitable.

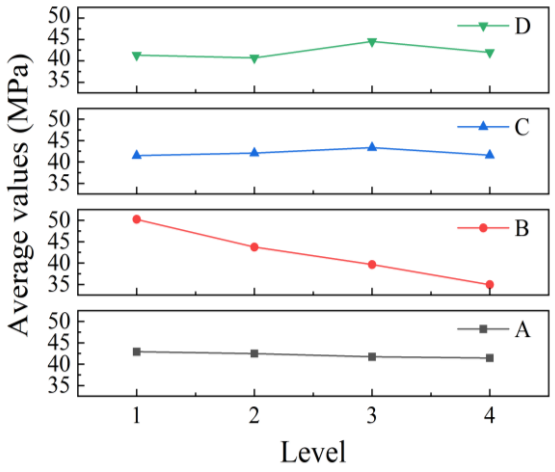

Fig. 3 The average value of the 90-day compressive strength factor of composite rubber mortar

4.1.3 Flexural strength

Table 7 shows the results of flexural strength at 7, 28 , and 90 days. The rubber content has the most significant effect on the flexural strength at all curing ages. The impact of each factor on the 7-day flexural strength is ranked as B>A>D>C; on the 28-day flexural strength is ranked as B>A>C>D; and on the 90-day flexural strength is ranked as B>D>C>A.

Table 6. Results of the range analysis for the compressive strength

Projects	7-day				28-day				90-day			
	Factor A	Factor B	Factor C	Factor D	Factor A	Factor B	Factor C	Factor D	Factor A	Factor B	Factor C	Factor D
Kavg value	27.15	31.95	26.28	27.23	37.88	37.80	36.52	36.25	42.90	50.20	41.48	41.33
	25.75	27.33	26.32	24.88	38.73	31.85	36.55	41.78	42.48	43.73	42.08	40.70
	27.27	24.35	27.23	27.05	35.90	42.80	40.48	33.65	41.70	39.65	43.37	44.55
	25.40	21.95	25.75	26.43	36.58	36.63	35.52	37.40	41.45	34.95	41.46	41.95
Optimum level	3	1	3	1	2	3	3	2	1	1	3	3
R	1.87	10.00	1.47	2.35	2.82	10.95	4.95	8.13	1.45	15.25	1.90	3.85

The range analysis of flexural strength revealed that the R-values of all factors consistently increased

from 7 to 90 days, indicating that the negative effect of rubber on flexural strength and the positive effects of fly ash and silica fume were progressively enhanced with hydration time. Fly ash and silica fume synergistically optimize the matrix structure through pozzolanic reactions, compensating for the weak interfacial zones of rubber while continuously enhancing flexural strength with curing age [22].

Fig. 4 shows the average value of the 90-day flexural strength of composite rubber mortar. The flexural strength decreases with increasing rubber particle size and content, while the combination of fly ash and silica fume in appropriate content is conducive to the enhancement of the flexural strength of mortar. For instance, as the rubber content increased from 5% to 20%, the 90-day flexural strength decreased by 27.4%. This is mainly attributed to the increase in porosity of the specimen matrix due to the incorporation of rubber, increasing of internal voids in the matrix, thus reducing the flexural strength of the specimen [23]. Since rubber incorporation reduces the flexural strength of specimens, fly ash and silica fume were jointly incorporated to leverage their strength-enhancing effects. Range analysis results indicate that while increased rubber particle size and dosage synergistically decrease flexural strength, silica fume absorbs $Ca(OH)_2$ during hydration to generate additional C-S-H gel, forming a denser structure that ultimately enhances flexural strength [24]. At the same time, the incorporation of fly ash can reduce the porosity and improve the pore structure, making the specimen matrix more complete and dense internally. However, the enhancement effect of the two on the strength will be affected by the fly ash content and the age of maintenance.

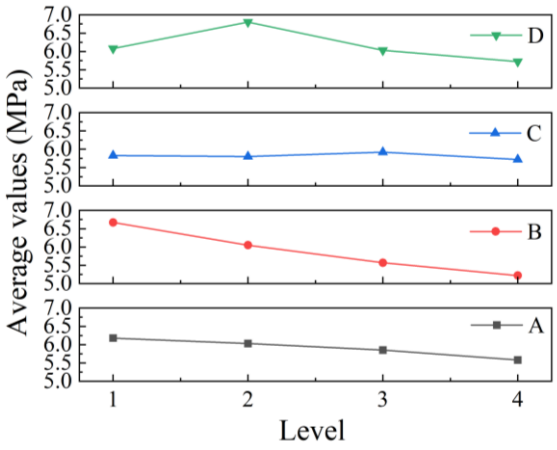

Fig. 4 The average value of the 90-day flexural strength factor of composite rubber mortar

4.1.4 Flexural-compression ratio

Table 8 shows the results of the range analysis of the flexural-compression ratio at 7, 28, and 90 days. It can be seen that the influence of each factor on the 7-day flexural-compression ratio is ranked as B>A>C>D, B>C>D>A for 28-day specimens, and B>D>C>A for 90-day specimens.

Table 7. R-values and optimal levels of range analysis of flexural strength at 7, 28, and 90 days

Age (day)	R				Optimum level			
	Factor A	Factor B	Factor C	Factor D	Factor A	Factor B	Factor C	Factor D
7	0.60	1.45	0.28	0.35	3	1	4	1
28	0.63	2.08	0.43	0.20	1	1	2	4
90	0.67	2.13	0.65	0.93	1	1	3	2

Table 8. Results of the range analysis for the flexural-compression ratios

Projects	7-day				28-day				90-day			
	Factor A	Factor B	Factor C	Factor D	Factor A	Factor B	Factor C	Factor D	Factor A	Factor B	Factor C	Factor D
Kavg value	0.192	0.173	0.188	0.196	0.199	0.184	0.197	0.203	0.238	0.215	0.225	0.227
	0.186	0.185	0.185	0.195	0.202	0.193	0.187	0.201	0.230	0.219	0.225	0.235
	0.184	0.192	0.193	0.174	0.196	0.206	0.206	0.187	0.219	0.233	0.219	0.225
	0.183	0.197	0.179	0.185	0.191	0.205	0.198	0.196	0.215	0.238	0.236	0.218
Optimum level	1	4	3	1	2	3	3	1	1	4	4	2
R	0.023	0.027	0.017	0.013	0.011	0.022	0.019	0.016	0.009	0.024	0.015	0.022

Range analysis revealed that rubber content maintained the most significant influence on the flexural-compression ratio, as evidenced by its consistently highest R-values (0.027, 0.022, and 0.024 for 7, 28, and 90 days, respectively). At 28- and 90-day ages, both fly ash and silica fume showed significantly higher R values than rubber particle size, confirming that the structural enhancement effect of mineral admixtures becomes progressively pronounced with extended curing. The underlying mechanisms reveal that: 1) rubber content primarily governs the density of interfacial weak zones, while 2) fly ash and silica fume improve matrix compactness through continuous pozzolanic reactions.

The flexural-compressive ratio is an indicator reflecting the deformation resistance, or toughness, of mortar. A higher flexural-compressive ratio indicates better toughness and crack resistance of the mortar [25]. Fig. 5 shows the average value of the 90-day flexural-compressive ratio at different levels. It can be observed that the smaller the rubber particle size, the higher the rubber content of 5%, and greater the flexural-compression ratio of the composite rubber mortar. When the rubber content increased from 5% to 20%, the flexural-compressive ratio of the composite rubber mortar at 90-day increased by 10.70%, compared with the OM group (flexural-compression ratio of 0.19) increased by 25.26%. This improvement can be attributed to the excellent elasticity and toughness of the rubber particles, which effectively absorb and dissipate a portion of the energy, thereby reducing stress concentrations within the specimen. This, in turn, enhances the internal stability and integrity of the matrix, ultimately leading to improved toughness [26]. Fly ash and silica fume fully exerted their “filling effect” and “pozzolanic effect”, significantly reducing the porosity of cementitious materials and producing a denser hydration product system. These microstructural improvements enhanced the homogeneity and compactness of the mortar, thereby effectively increasing the crack resistance and toughness of the specimens [27].

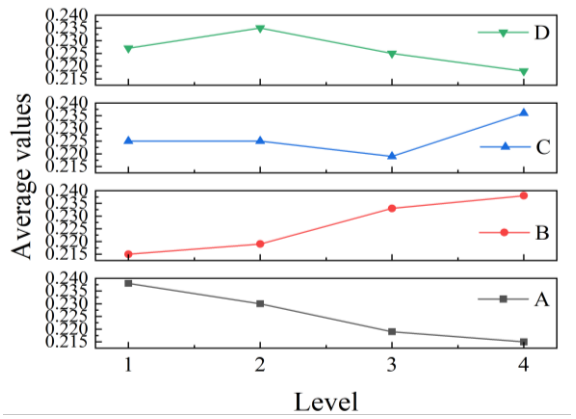

Fig. 5 The average value of the 90-day flexural-compressive ratio factor of composite rubber mortar

4.2 Variance analysis

Given that range analysis cannot distinguish between errors caused by variations in test conditions and those arising from random factors, nor quantify the statistical significance of factor-level effects. Analysis of variance (ANOVA) was employed to overcome these limitations in evaluating the fluidity, compressive strength, flexural strength, and flexural-compression ratio of composite rubber mortar. The results are shown in Table 9. The impact of each factor on fluidity is ranked as D>B>A>C; on 28-day compressive strength as B>D>C>A; on 28-day flexural strength as B>A>C>D; and on 28-day flexural-compression ratio as B>C>D>A. The results of the variance analysis are in agreement with those of the range analysis, which indicates the reliability of the results of the range analysis.

4.3 TOPSIS and Cost analysis

4.3.1 TOPSIS analysis

Technique for order preference by similarity to ideal solution (TOPSIS) has been widely used as an effective multi-objective decision-making method to determine the combined performance of different conflicting aspects [28]. To determine the optimum combination of ratios for the test, the fluidity, compressive strength, flexural strength, and flexural-compression ratio of the composite rubber mortar, were analyzed by TOPSIS synthesis and the results are shown in Table 10. The optimal combination of four indices (fluidity, compressive strength, flexural strength, and flexural-compression ratio, as shown in Tables 5~8) at three ages (7, 28, and 90 days) is A1B1C4D2. The composite rubber mortar achieves the best overall performance when the rubber particle size is 150 mesh, the rubber content is 5 %, the fly ash content is 20 %, and the silica fume content is 5 %.

4.3.2 Cost analysis

Partial substitution of solid waste in building materials significantly reduces natural resource consumption and carbon emissions, delivering dual economic and environmental benefits [29]. According to the China Sand & Stone Association (CSSA), the national manufactured sand (M-sand) production reached 12.92 billion tonnes in 2024. TOPSIS multi-criteria decision analysis determined an optimal rubber replacement rate of 5%, conserving approximately 0.646 billion tonnes of aggregate resources. At the 2024 market average price of $11.97 per tonne for M-sand (China Building Materials Federation), this yields direct raw material savings of $7.74 billion. Concurrently, this approach reduces resource recovery costs for waste tires while mitigating environmental externalities associated with end-of-life tire management.

Per China Cement Network data, national cement output reached 1.825 billion tonnes that year. Applying a composite replacement system (20% FA, 5% SF) optimized by TOPSIS reduces cement usage by 456 million tonnes. Based on the 2024 average cement production cost of $55.67 per tonne (China Cement Association), this cuts material expenditures by $25.38 billion. Synergistic utilization of FA ($16.90 per tonne) and SF ($104.23 per tonne) achieves a 9.6% unit cost reduction for composite cementitious materials. The unit cost reduction rate was calculated using the following formula:

$$\mathrm{Cost}_{\mathrm{comp}} = 0.75C_{cem} + 0.2C_{FA} + 0.05C_{SF} \quad (1)$$

$$\eta = (1 - Cost_{comp} / C_{cem}) \times 100\% \quad (2)$$

Where: $\mathrm{Cost}_{\mathrm{comp}}$, C_{cem}, C_{FA}, and C_{SF} denote the weighted average unit cost of composite cementitious materials, unit price of cement, unit price of fly ash, and unit price of silica fume, respectively.

This optimal composite simultaneously reduces CO_2 emissions by approximately 0.388 billion tonnes, generating carbon trading revenues equivalent to $3.77 billion (based on the 2024 daily minimum price of $9.72 per tonne from Shanghai Environment and Energy Exchange). The synergistic incorporation of rubber, fly ash, and silica fume maximizes solid waste utilization while maintaining the mechanical properties of mortar. This approach provides the construction materials sector with a technological pathway that integrates economic viability with low-carbon benefits [30].

4.4 Microstructure

This study investigated the pore structure characteristics and pore size distribution variations in specimens incorporating rubber, fly ash, and silica fume, and their effects on macroscopic properties. To elucidate the underlying mechanisms, MIP and SEM analyses were conducted on specimens cured for 28 and 90 days.

4.4.1 MIP analysis

Table 11 shows the MIP results of composite rubber mortar at 28-day. It can be seen that: A2B4C3D2 exhibits the maximum porosity, while A4B4C4D4 has the largest average pore diameter. Conversely, the porosity and average pore diameter of A3B1C3D1 are the lowest. This may be attributed to the particle grading of the quaternary system formed by rubber, fly ash, silica fume, and cementin A3B1C3D1 is better, and the matrix is more denser.

Table 9. Variance analysis for mechanical properties of composite rubber mortar

Projects	Factor	Sum of squares	Degrees of freedom	Mean square	F-value	Significance
Fluidity / mm	A	390	3	130	13.574	0.05*
	B	466	3	155	16.217	0.01*
	C	262	3	87	9.122	/
	D	5586	3	1862	194.304	0.001**
Compressive strength/ MPa	A	242.617	3	6.457	0.510	/
	B	19.372	3	80.872	6.389	0.001**
	C	57.562	3	19.187	1.516	/
	D	137.827	3	45.942	3.629	0.05*
Flexural strength/ MPa	A	1.040	3	0.350	24.76	0.01*
	B	2.710	3	0.900	64.64	0.001**
	C	0.360	3	0.120	8.64	0.05*
	D	0.160	3	0.050	3.87	/
Flexural-compression ratio	A	0.000	3	0.000	0.38	/
	B	0.001	3	0.000	1.92	0.01*
	C	0.001	3	0.000	1.00	/
	D	0.001	3	0.000	0.88	/

*Note: ** indicates highly significant effect; * indicates significant effect; / indicates insignificant effect.*

Additionally, the rubber content in A3B1C3D1 (5%) is smaller than in A4B4C4D4 (20%), and the fly ash and silica fume are added in moderate amounts so the porosity and the average pore diameter in A4B4C4D4 are larger than those in A3B1C3D1. Reducing the rubber particle size and content can collectively increase the content of gel pores (<20 nm) and small capillary pores (20 ~50 nm), while decreasing the content of capillary pores (50~100 nm), transition pores (100~1000 nm) and large pores (>1000 nm). This is because the addition of an appropriate amount of silica fume can react with OH^- to generate a large number of C-S-H gels, which, together with fly ash, can fill the voids between cement particles and aggregates, thereby refining the pore structure [31]. Fig. 6 shows the differential curve of the pore size distribution of composite rubber mortar at 28-day. It can be seen that the most critical pore diameter of the composite rubber mortar falls within the range of 20~50 nm. The most critical pore diameters are in the order of A3B1C3D1＜A1B4C1D3＜A2B4C3D2＜A4B4C4D4, and the rubber content of 5% is the smallest in A3B1C3D4, while the rubber content of 5% is the same for A1B4C1D3, A2B4C3D2, and A4B4C4D4, which are all 20%. Samples A1B4C1D3, A2B4C3D2, and A4B4C4D4 all have the same rubber content of 20%. This shows that when rubber content is constant, the critical pore diameter increases with rubber particle size. Fly ash and silica fume exert a less significant impact on the critical pore diameter compared with the combined effect of rubber particle size and content.

Table 10. Comprehensive evaluation results of TOPSIS method for composite rubber mortar

Specimen	Positive ideal solution distance D+	Negative ideal solution distance D-	Relative proximity C	Sorting results
A1B1C4D2	0.202	58.113	0.997	#
A1B2C3D1	10.115	48.054	0.826	-
A1B3C2D4	30.121	28.030	0.482	-
A1B4C1D3	58.122	0.103	0.002	-
A2B1C2D3	43.019	15.228	0.261	-
A2B2C1D4	45.021	13.233	0.227	-
A2B3C4D1	2.500	58.017	0.959	-
A2B4C3D2	13.240	45.019	0.773	-
A3B1C3D4	31.016	27.222	0.467	-
A3B2C4D3	40.026	18.155	0.312	-
A3B3C1D2	4.730	54.016	0.919	-
A3B4C2D1	15.194	43.023	0.739	-
A4B1C1D1	17.047	41.113	0.707	-
A4B2C2D2	8.139	50.055	0.860	-
A4B3C3D3	58.034	2.400	0.040	-
A4B4C4D4	58.057	1.404	0.024	-

Note: # indicates the optimal combination.

Table 11. MIP test results of composite rubber mortar at 28-day

Specimen	Large pore/nm	Transition pore/nm	Capillary pore/nm	Small capillary pore/nm	Gel pore /nm	Porosity/%	Average pore diameter/nm	Critical pore diameter/nm
A1B4C1D3	0.50	0.68	0.31	0.45	1.80	17.61	14.09	32.38
A2B4C3D2	0.62	0.80	0.36	0.51	1.90	18.53	14.58	40.25
A3B1C3D1	0.51	0.69	0.30	0.42	1.66	16.63	13.54	26.30
A4B4C4D4	0.56	0.67	0.32	0.45	1.71	16.92	15.02	40.26

Fig. 7 (a) and (b) illustrate the relationship between porosity and strength at 28-day. As can be seen from the figures, A3B1C3D1 exhibits the lowest porosity, resulting in the highest compressive and flexural strengths.

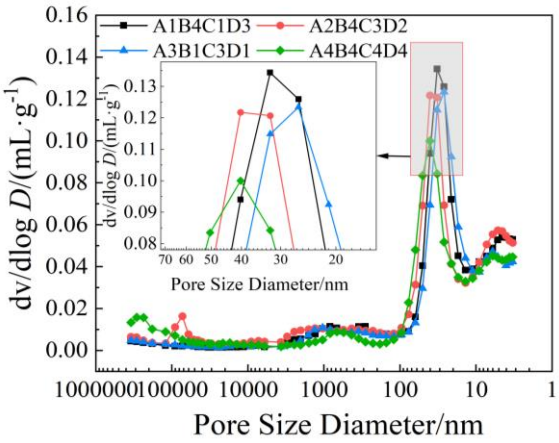

Fig. 6 Differential curve of 28-day pore size distribution of composite rubber mortar

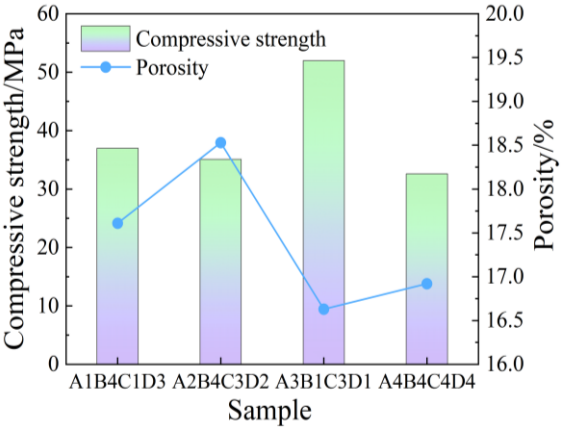

(a)

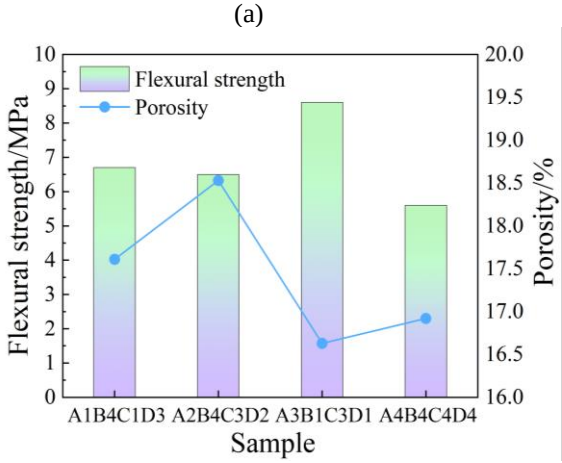

(b)

Fig. 7 Relationship between porosity and compressive and flexural strengths: (a) Porosity and 28-day compressive strength; (b) Porosity and 28-day flexural strength

Conversely, A2B4C3D2 has the highest porosity, yet its compressive and flexural strengths are not the lowest. Surprisingly, A4B4C4D4, with a porosity second only to A3B1C3D1, demonstrates the lowest compressive and flexural strengths. This may be attributed to the fact that A4B4C4D4 contains the largest rubber particle size and content among the four composite mortars, and both its average pore diameter and most critical pore diameter are the largest. Given that the average pore diameter is negatively correlated with the compressive strength, A4B4C4D4 exhibits the lowest strength. The smaller pores in groups A3B1C3D1 and A4B4C4D4 may be attributed to their fly ash content exceeding 15%. The low early-stage reactivity of fly ash was followed by enhanced participation in later reactions, yielding additional hydration products. These hydration products refined the pore structure of the composite rubber mortar, resulting in a denser microstructure and significantly reduced porosity [32].

4.4.2 SEM analysis

At 28 and 90 days, it was observed that some incompletely hydrated fly ash, silica fume particles, and tiny fissures and pores exist within the matrix of A1B4C1D3, A2B4C3D2, A3B1C3D1, and A4B4C4D4, as shown in Figs. 8 (a)~(h). This phenomenon may be due to: 1) The tested groups incorporated relatively high dosages of silica fume ($SiO_2 \geqslant 96\%$). Its ultra-high specific surface area substantially increased water demand for hydration. By 90 days of curing, the majority of silica fume had been consumed through pozzolanic reactions, forming C-S-H gel [33]. However, residual unreacted silica fume particles intensely adsorbed pore solution moisture, inducing capillary tension within the surrounding cementitious matrix. This led to localized autogenous shrinkage stress. Stress concentration at particle-matrix interfaces readily initiated microcracks, consequently compromising the strength of the composite rubber mortar. 2) Specimens A1B4C1D3, A2B4C3D2, A3B1C3D1, and A4B4C4D4 incorporate high fly ash replacement levels for cement. However, fly ash exhibits low reactivity, participating minimally in early-stage hydration. Its pozzolanic reaction primarily occurs during middle to late stages. Concurrently, excessive silica fume content depletes alkaline substances in the mortar matrix. This dual effect leads to incomplete hydration of cementitious materials.

Specifically, at 28-day, fly ash that has not yet fully hydrated filled in the pores of the matrix, giving full play to its micro aggregate effect, making the matrix denser, as shown in Figs. 8 (a), (b), (c). The mixture of fly ash and silica fume plays a complementary role. Specimen A4B4C4D4 incorporates 20% rubber particles with 10 mesh gradation. Both the rubber particles and content exceed those in A1B4C1D3, A2B4C3D2, and A3B1C3D4, resulting in increased matrix porosity that diminishes the compensatory effect of fly ash and silica fume on strength development.

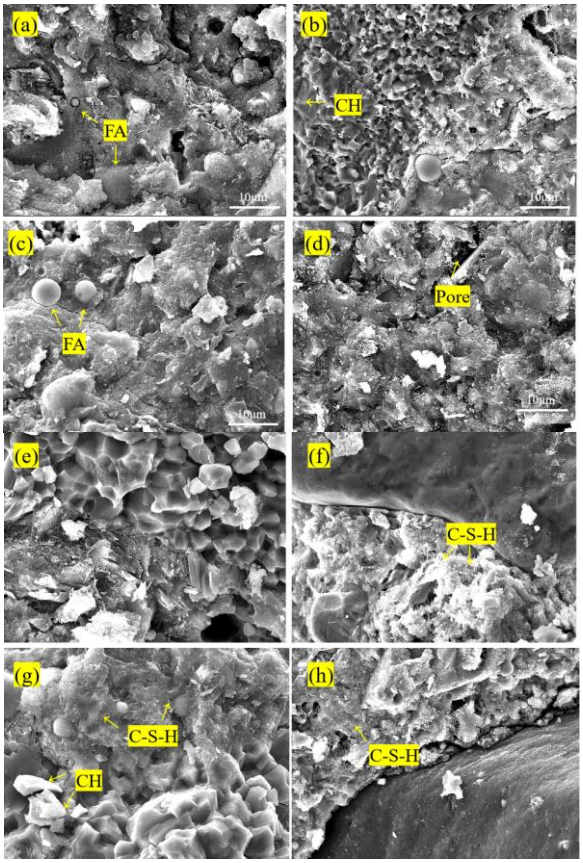

Fig. 8 SEM images: (a) A1B4C1D3 at 28-day; (b) A2B4C3D2 at 28-day; (c) A3B1C3D1 at 28-day: (d) A4B4C4D4 at 28-day; (e) A1B4C1D3 at 90-day; (f) A2B4C3D2 at 90-day; (g) A3B1C3D1 at 90-day; (h) A4B4C4D4 at 90-day

At 90-day curing, abundant fibrillar C-S-H gels and scarce hexagonal $Ca(OH)_2$ crystals were observed, with unreacted fly ash and silica fume particles tightly encapsulated by dense C-S-H gels, as shown in Fig. 8 (g). This microstructural evolution confirms substantial pozzolanic reactions, constituting the primary mechanism for the superior mechanical strength in this group. Specimens A1B4C1D3 and A2B4C3D2 demonstrate predominantly amorphous hydration products, as shown in Fig. 8 (e) and (f), respectively. The complete encapsulation of fly ash and silica fume by C-S-H gels indicates advanced pozzolanic reactions. This microarchitecture effectively refines capillary pores, thereby enhancing both compressive and flexural strengths. The interfacial zone between rubber particles and cement paste in A4B4C4D4 is clearly observed, as shown in Fig. 8 (h). The chemically inert rubber fails to establish chemical bonding with cementitious matrices, resulting in pronounced wall effects. The porous and discontinuous interface morphology creates mechanical weak points, ultimately compromising the 90-day compressive and flexural strengths.

5. CONCLUSIONS

1）The effects of rubber particle size and content, fly ash content, and silica fume content on the fluidity and mechanical properties of rubber mortar were investigated with the help of L16 (4×4) orthogonal experiment. By both range analysis and variance analysis in orthogonal experiments, it was found that the content of silica fume had the most significant influence on the fluidity of composite rubber mortar. The content of rubber content had the most significant influence on the compressive strength, flexural strength, and flexural-compression ratio of composite rubber mortar. Neither rubber particle size nor the content of fly ash were significant factors.

2）Based on the TOPSIS method, the optimal combination of the four indexes of comprehensive fluidity, compressive strength, flexural strength, and flexural-compression ratio is A1B1C4D2. That is, the best comprehensive performance of composite rubber mortar is achieved when the rubber particle size is 150 mesh, the rubber content of 5%, the fly ash content of 20% ,and the silica fume content of 5%.

3）Incorporating fly ash and silica fume can mitigate the weakened interfacial transition zone caused by rubber addition. Fly ash and silica fume can optimize the pore structure of the composite mortar and enhance its mechanical properties, which in turn can alleviate the weakening degree of the rubber on the strength of the composite rubber mortar.

6. ACKNOWLEDGMENTS

This study was funded by the Guizhou Provincial Basic Research Program (Natural Science) (No. QKHJC-ZK [2023]YB261).

7. REFERENCES

[1] Wang Q. Z., Chen Z. D., Lin K. P., & Wang C. H., Estimation and analysis of energy conservation and emissions reduction effects of warm-mix crumb rubber-modified asphalts during construction period. Sustainability, 10(12), 2018, 4521. https://doi.org/10.3390/su10124521.

[2] Roychand R., Gravina R. J., Zhuge Y., Ma X., Youssf O., & Mills J. E., A comprehensive review on the mechanical properties of waste tire rubber concrete. Construction and Building Materials, Vol. 237, 2020, 117651. https://doi.org/10.1016/j.conbuildmat.2019.117651.

[3] Liu F., Zheng W., Li L., Feng W., & Ning G., Mechanical and fatigue performance of rubber concrete. Construction and Building Materials,

Vol. 47, 2013, pp. 711-719.
https://doi.org/10.1016/j.conbuildmat.2013.05.055.

[4] Bala A., & Gupta S., Thermal resistivity, sound absorption and vibration damping of concrete composite doped with waste tire Rubber: A review. Construction and Building Materials, Vol. 299, 2021, 123939.
https://doi.org/10.1016/j.conbuildmat.2021.123939.

[5] Li Y., Zhang S., Wang R., & Dang F., Potential use of waste tire rubber as aggregate in cement concrete–A comprehensive review. Construction and Building Materials, Vol. 225, 2019, pp. 1183-1201.
https://doi.org/10.1016/j.conbuildmat.2019.07.198.

[6] Bu C., Zhu D., Liu L., Lu X., Sun Y., Yu L., OuYang Y., Cao X., & Wang F., Research progress on rubber concrete properties: a review. Journal of Rubber Research, 25(2), 2022, pp. 105-125.
https://doi.org/10.1007/s42464-022-00161-8.

[7] Choudhary R., Gupta R., & Nagar R., Impact on fresh, mechanical, and microstructural properties of high strength self-compacting concrete by marble cutting slurry waste, fly ash, and silica fume. Construction and Building Materials, Vol. 239, 2020, 117888.
https://doi.org/10.1016/j.conbuildmat.2019.117888.

[8] Saing Z., Mairuhu D., & Tumpu M., Characteristics of asphalt concrete wearing course mix incorporating recycled tire rubber as an additive. International Journal of GEOMATE, 26(115), 2024, pp. 34-43.
https://doi.org/10.21660/2024.115.4195.

[9] Hilal N. N., Hardened properties of self-compacting concrete with different crumb rubber size and content. International Journal of Sustainable Built Environment, 6(1), 2017, pp. 191-206.
https://doi.org/10.1016/j.ijsbe.2017.03.001.

[10] ZHU P. Y., WAN H. L., ZHU Y., & Gu W. H., Experimental study on mechanical properties of hybrid fiber rubber concrete based on orthogonal experiment. Composites Science and Engineering, 12, 2021, pp. 73-77.
DOI:10.19936/j.cnki.2096-8000.20211228.011.
朱鹏宇, 万后林, 朱叶, 顾文虎. 基于正交试验法的混杂纤维橡胶混凝土力学性能试验研究. 复合材料科学与工程, 2021, (12): pp.73-77.
DOI:10.19936/j.cnki.2096-8000.20211228.011.

[11] Gupta T., Sharma R. K., & Chaudhary S., Impact resistance of concrete containing waste rubber fiber and silica fume. International Journal of Impact Engineering, Vol. 83, 2015, pp. 76-87.
https://doi.org/10.1016/j.ijimpeng.2015.05.002.

[12] Guo J., Zhang Z., Wu J., Wang H., Zhang P., Wang K., Meng Q., & Xu H., Early-age mechanical characteristics and microstructure of concrete containing mineral admixtures under the environment of low humidity and large temperature variation. Materials, 67(3), 2021, 5085.
https://doi.org/10.3390/ma14175085.

[13] ZHANG J. S., TANG Y. L., ZHAN J. J., & PANG J. Y., Study on creep properties and microscopic mechanism of silica fume rubber/cement mortar. Journal of Building Materials, 41(08), 2024, pp. 1-11.
DOI:10.13801/j.cnki.fhclxb.20240008.004.
张金松, 唐雨轮, 占佳佳&庞建勇, 动静加载下微硅粉-橡胶/水泥砂浆的力学性能. 复合材料学报, 2024, 41(08): pp. 4287-4298.
DOI:10.13801/j.cnki.fhclxb.20240008.004.

[14] Nežerka V., Bílý P., Hrbek V., & Fládr J., Impact of silica fume, fly ash, and metakaolin on the thickness and strength of the ITZ in concrete. Cement and concrete composites, Vol. 103, 2019, pp. 252-262.
https://doi.org/10.1016/j.cemconcomp.2019.05.012.

[15] Arshad M. T., Ahmad S., Khitab A., & Hanif A., Synergistic use of fly ash and silica fume to produce high-strength self-compacting cementitious composites. Crystals, 11(8), 2021, 915..
https://doi.org/10.3390/cryst11080915.

[16] Rogojsz G., & Rudnicki T., Influence of Mineral Additives on Strength Properties of Standard Mortar. Materials, 17(16), 2024, 4158.
https://doi.org/10.3390/ma17164158.

[17] LIU Y. W., ZHANG Z. H., SHI C. J., LI N., & LEI L., Influence of Silica Fume on Performance of High-Strength Geopolymer. Journal of the Chinese Ceramic Society, 48(11), 2020, pp. 1689-1699.
DOI:10.14062/j.issn.0454-5648.20200234.
刘翼玮, 张祖华, 史才军, 李宁&雷龙, 硅灰对高强地聚物胶凝材料性能的影响. 硅酸盐学报, 2020, 48(11): pp. 1689-1699.
DOI:10.14062/j.issn.0454-5648.20200234.

[18] Xiong Z., Tang Z., He S., Fang Z., Chen Z., Liu F., & Li L., Analysis of mechanical properties of rubberised mortar and influence of styrene–butadiene latex on interfacial behaviour of rubber–cement matrix. Construction and Building Materials, Vol. 300, 2021, 124027.
https://doi.org/10.1016/j.conbuildmat.2021.124027.

[19] Li X., Ling T. C., & Mo K. H., Functions and impacts of plastic/rubber wastes as ecofriendly aggregate in concrete–A review. Construction and building materials, Vol. 240, 2020, 117869.
https://doi.org/10.1016/j.conbuildmat.2019.117869.

[20] Youssf O., Hassanli R., & Mills J. E.,

Mechanical performance of FRP-confined and unconfined crumb rubber concrete containing high rubber content. Journal of Building Engineering, Vol. 11, 2017, pp. 115-126. https://doi.org/10.1016/j.jobe.2017.04.011.

[21] Majhi R. K., Padhy A., & Nayak A. N., Performance of structural lightweight concrete produced by utilizing high volume of fly ash cenosphere and sintered fly ash aggregate with silica fume. Cleaner Engineering and Technology, 3, 2021, 100121. https://doi.org/10.1016/j.clet.2021.100121.

[22] Alaloul W. S., Musarat M. A., Haruna S., Law K., Tayeh B. A., Rafiq W., & Ayub S., Mechanical properties of silica fume modified highvolume fly ash rubberized self-compacting concrete. Sustainability, Vol. 13, 2021, 5571. https://doi.org/10.3390/su13105571.

[23] Zhai S., Zhou X., Zhang Y., Pang B., Liu G., Zhang L., Yang L., Liu Z., & Liu L., Effect of multifunctional modification of waste rubber powder on the workability and mechanical behavior of cement-based materials. Construction and Building Materials, Vol. 363, 2023, 129880. https://doi.org/10.1016/j.conbuildmat.2022.129880.

[24] Gu B., Li Q., Li C., Zhao P., Hou P., Chen H., Wang Y., Zhao P., & Cheng X., Optimization design of ultra-fine supplementary cementitious materials ultra-high performance concrete mix proportion based on orthogonal experiment. Construction and Building Materials, Vol. 453, 2024, 139018. https://doi.org/10.1016/j.conbuildmat.2024.139018.

[25] Xu Y., & Yang R., Dynamic mechanics and damage evolution characteristics of rubber cement mortar under different curing humidity levels. Journal of Materials in Civil Engineering, 32(10), 2020, 04020309. https://doi.org/10.1061/(ASCE)MT.1943-5533.0003351.

[26] Feng W., Liu F., Yang F., Jing L., Li L., Li H., & Chen L., Compressive behaviour and fragment size distribution model for failure mode prediction of rubber concrete under impact loads. Construction and Building Materials, Vol. 273, 2021, 121767. https://doi.org/10.1016/j.conbuildmat.2020.121767.

[27] Lakhiar M. T., Kong S. Y., Bai Y., Susilawati S., Zahidi I., Paul S. C., & Raghunandan M. E., Thermal and mechanical properties of concrete incorporating silica fume and waste rubber powder. Polymers, 14(22), 2022, 4858.. https://doi.org/10.3390/polym14224858.

[28] Wang Y., Zhong K., He J., & Kang Y., Numerical study on balancing air quality in streets and adjacent neighborhoods using combined porous media model and TOPSIS method. Building and Environment, 2025, 113219. https://doi.org/10.1016/j.buildenv.2025.113219.

[29] Cuong N. H., Workability, mechanical and durability investigations on self-compacting concrete with high fly ash content and recycled fine aggregate. International Journal of GEOMATE, 26(118), 2024, pp. 96-104. https://doi.org/10.21660/2024.118.4409.

[30] Yohans S., Parea R. R., Ermitha A., & Miswar T., Mechanical properties of foamed concrete (FC) using high-volume fly ash. International Journal of GEOMATE, 26(118), 2024, pp. 141–148. https://doi.org/10.21660/2024.118.g13323.

[31] Zhagifarov A., Talal A., Akhmetov D., Suzev N., & Kolesnikova I., Effectiveness of Road Slabs Produced Using Microsilica and Fiber Quality Improvement. International Journal of GEOMATE, 28(126), 2025, 16-24. https://doi.org/10.21660/2025.126.4335.

[32] Sunarno Y., Rangan P. R., Ampangallo B. A., Aryadi A., Nelfia L. O., & Rinanti A., The influence of chemical admixture types on the mechanical properties of concrete with 100% fly ash substitution. International Journal of GEOMATE, 28(129), 2025, pp. 138-145. https://doi.org/10.21660/2025.129.g14383.

[33] Bai W., Lu X., Guan J., & Yuan C., Experimental study on uniaxial compression mechanical properties of recycled concrete with silica fume considering the effect of curing age. Construction and Building Materials, 350, 2022, 128758. https://doi.org/10.1016/j.conbuildmat.2022.128758.